AD-A154 962 EQUITORIAL SCINTILLATIONS: ADVANCES SINCE ISEA-6(U) 1/1
EMMANUEL COLL BOSTON MA S BASU JAN 85 SCIENTIFIC-1
AFGL-TR-85-0014 F19628-84-K-0003

UNCLASSIFIED F/G 4/1 NL

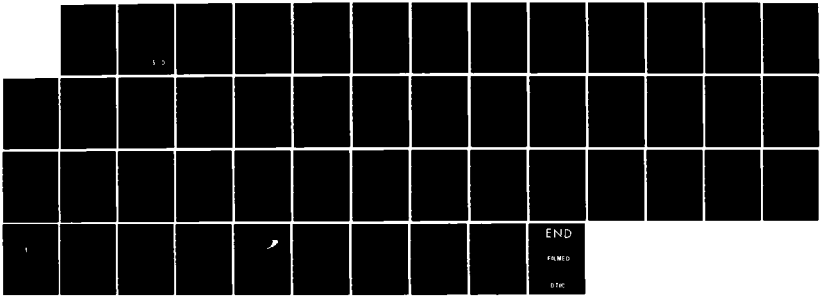

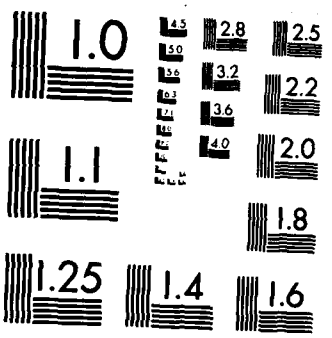

AFGL-TR-85-0014

EQUATORIAL SCINTILLATIONS: ADVANCES SINCE ISEA-6

Sunanda Basu
Santimay Basu

Emmanuel College
400 The Fenway
Boston, Massachusetts 02115

Scientific Report No. 1

January 1985

Approved for public release; distribution unlimited

AIR FORCE GEOPHYSICS LABORATORY
AIR FORCE SYSTEMS COMMAND
UNITED STATES AIR FORCE
HANSCOM AFB, MASSACHUSETTS 01731

"This technical report has been reviewed and is approved for publication"

HERBERT E. WHITNEY
Contract Manager
Ionospheric Effects Branch

HERBERT C. CARLSON, Chief
Ionospheric Effects Branch
Ionospheric Physics Division

FOR THE COMMANDER

ROBERT A. SKRIVANEK
Director
Ionospheric Physics Division

This report has been reviewed by the ESD Public Affairs Office (PA) and is releasable to the National Technical Information Service (NTIS).

Qualified requestors may obtain additional copies from the Defense Technical Information Center. All others should apply to the National Techncial Information Service.

If your address has changed, or if you wish to be removed from the mailing list, or if the addressee is no longer employed by your organization, please notify AFGL/DAA, Hanscom AFB, MA 01731. This will assist us in maintaining a current mailing list.

UNCLASSIFIED

SECURITY CLASSIFICATION OF THIS PAGE

REPORT DOCUMENTATION PAGE

1a. REPORT SECURITY CLASSIFICATION Unclassified	1b. RESTRICTIVE MARKINGS None
2a. SECURITY CLASSIFICATION AUTHORITY N/A	3. DISTRIBUTION/AVAILABILITY OF REPORT Approved for public release; distribution unlimited
2b. DECLASSIFICATION/DOWNGRADING SCHEDULE N/A	
4. PERFORMING ORGANIZATION REPORT NUMBER(S) Emmanuel College 400 The Fenway, Boston, MA 02115	5. MONITORING ORGANIZATION REPORT NUMBER(S) AFGL-TR-85-0014
6a. NAME OF PERFORMING ORGANIZATION Air Force Geophysics Lab 6b. OFFICE SYMBOL (If applicable) LIS	7a. NAME OF MONITORING ORGANIZATION
6c. ADDRESS (City, State and ZIP Code) Hanscom AFB MA 01731 Monitor: Herbert Whitney	7b. ADDRESS (City, State and ZIP Code)
8a. NAME OF FUNDING/SPONSORING ORGANIZATION Air Force Geophysics Lab. 8b. OFFICE SYMBOL (If applicable) LIS	9. PROCUREMENT INSTRUMENT IDENTIFICATION NUMBER F19628-84-K-0003
8c. ADDRESS (City, State and ZIP Code) Hanscom AFB MA 01731	10. SOURCE OF FUNDING NOS. PROGRAM ELEMENT NO.: 62101F PROJECT NO.: 4643 TASK NO.: AA WORK UNIT NO.: AC
11. TITLE (Include Security Classification) Equatorial Scintillations: Advances Since ISEA-6 (U)	
12. PERSONAL AUTHOR(S) Sunanda Basu and Santimay Basu	
13a. TYPE OF REPORT Scientific No. 1 13b. TIME COVERED FROM _____ TO _____	14. DATE OF REPORT (Yr., Mo., Day) January 1985 15. PAGE COUNT 46
16. SUPPLEMENTARY NOTATION Reprint	
17. COSATI CODES FIELD / GROUP / SUB. GR.	18. SUBJECT TERMS (Continue on reverse if necessary and identify by block number) Scintillation morphology, bubbles and sinusoidal irregularities; scintillation spectra

19. ABSTRACT (Continue on reverse if necessary and identify by block number)

Since the last equatorial aeronomy meeting in 1980, our understanding of the morphology of equatorial scintillations has advanced greatly due to more intensive observations at the equatorial anomaly locations in the different longitude zones. The unmistakable effect of the sunspot cycle in controlling irregularity belt width and electron concentration responsible for strong scintillation in the GHz range has been demonstrated. The fact that nighttime F-region dynamics is an important factor in controlling the magnitude of scintillations has been recognized by interpreting scintillation observations in the light of realistic models of total electron content at various longitudes. A hypothesis based on the alignment of the solar terminator with the geomagnetic flux tubes as an indicator of enhanced scintillation occurrence and another based on the influence of a transequatorial thermospheric neutral wind have been postulated to describe the observed longitudinal variation.

A distinct class of equatorial irregularities known as the bottomside sinusoidal (BSS) type has been identified. Unlike equatorial bubbles these irregularities occur in very large patches sometimes in excess of several thousand km in the E-W direction and are

20. DISTRIBUTION/AVAILABILITY OF ABSTRACT UNCLASSIFIED/UNLIMITED ☒ SAME AS RPT. ☐ DTIC USERS ☐	21. ABSTRACT SECURITY CLASSIFICATION Unclassified
22a. NAME OF RESPONSIBLE INDIVIDUAL Herbert E. Whitney	22b TELEPHONE NUMBER (Include Area Code) 617-861-3982 22c. OFFICE SYMBOL AFGL/LIS

DD FORM 1473, 83 APR EDITION OF 1 JAN 73 IS OBSOLETE.

Unclassified

SECURITY CLASSIFICATION OF THIS PAGE

associated with frequency spread on ionograms. Scintillations caused by such irregularities exist only in the VHF band, exhibit Fresnel oscillations in intensity spectra, and are found to give rise to extremely long durations (∿ several hours) of uninterrupted scintillations. These irregularities maximize during solstices so that in the VHF range, scintillation morphology at an equatorial station is determined by considering occurrence characteristics of both bubble type and BSS type irregularities.

The temporal structure of scintillations in relation to the in-situ measurements of irregularity spatial structure within equatorial bubbles has been critically examined. A two-component irregularity spectrum with a shallow slope ($p_1 \sim 1.5$) at long scalelengths (> 1km) and steep slope ($p_2 \sim -3$) at shorter scalelengths has been found in both vertical and horizontal spectra. Phase and intensity scintillation modeling was found to be consistent with this two-component irregularity spectrum.

Finally, the information provided by the major experimental undertaking represented by Project Condor in the fields of daytime and nighttime scintillations and zonal irregularity drifts will be briefly outlined.

ABSTRACT

Since the last equatorial aeronomy meeting in 1980, our understanding of the morphology of equatorial scintillations has advanced greatly due to more intensive observations at the equatorial anomaly locations in the different longitude zones. The unmistakable effect of the sunspot cycle in controlling irregularity belt width and electron concentration responsible for strong scintillation in the GHz range has been demonstrated. The fact that nighttime F-region dynamics is an important factor in controlling the magnitude of scintillations has been recognized by interpreting scintillation observations in the light of realistic models of total electron content at various longitudes. A hypothesis based on the alignment of the solar terminator with the geomagnetic flux tubes as an indicator of enhanced scintillation occurrence and another based on the influence of a transequatorial thermospheric neutral wind have been postulated to describe the observed longitudinal variation.

A distinct class of equatorial irregularities known as the bottomside sinusoidal (BSS) type has been identified. Unlike equatorial bubbles these irregularities occur in very large patches sometimes in excess of several thousand km in the E-W direction and are associated with frequency spread on ionograms. Scintillations caused by such irregularities exist only in the VHF band, exhibit Fresnel oscillations in intensity spectra, and are found to give rise to extremely long durations (~ several hours) of uninterrupted scintilla-

tions. These irregularities maximize during solstices so that in the VHF range, scintillation morphology at an equatorial station is determined by considering occurrence characteristics of both bubble type and BSS type irregularities.

The temporal structure of scintillations in relation to the in-situ measurements of irregularity spatial structure within equatorial bubbles has been critically examined. A two-component irregularity spectrum with a shallow slope ($p_1 \sim 1.5$) at long scalelengths (>1 km) and steep slope ($p_2 \sim -3$) at shorter scalelengths has been found in both vertical and horizontal spectra. Phase and intensity scintillation modelling was found to be consistent with this two-component irregularity spectrum.

Finally, the information provided by the major experimental undertaking represented by Project Condor in the fields of daytime and nighttime scintillations and zonal irregularity drifts will be briefly outlined.

INTRODUCTION

The subject of nighttime equatorial F-region irregularities has received a tremendous amount of attention in the last decade. Much new information has become available on multi-technique experiment, theory and numerical simulation of these irregularities. In this rapidly developing field, reviews having various experimental and theoretical orientations followed in quick succession (Farley, 1974; Aarons, 1977, 1982; Basu and Kelley, 1977, 1979; Fejer and Kelley, 1980; Ossakow, 1979, 1981; Kelley and McClure, 1981; Basu and Basu, 1981; Yeh and Liu, 1982). In particular, many of the above have dealt at length with the various aspects of equatorial scintillations. Among the reviews mentioned above, three, namely those by Basu and Basu (1981), Kelley and McClure (1981) and Ossakow (1981), were presented at the sixth ISEA in Puerto Rico.

We shall divide this review under four broad headings and try to bring the reader the latest information on each of these topics:

i) the latitudinal variation of scintillation

ii) the longitudinal variation of scintillation

iii) the structure of equatorial irregularities measured in-situ

iv) the modelling of equatorial scintillations based on such structure.

i) LATITUDE VARIATION

Since the last equatorial aeronomy meeting in 1980, our knowledge regarding the morphology of equatorial scintillations has advanced greatly due to the establishment of many observing sites, particularly near the crest of the equatorial anomaly. The unmistakable effect of the sunspot cycle in controlling irregularity belt width and electron concentration responsible for intense scintillation has been demonstrated by utilizing measurements made near the anomaly crest, namely, at Ascension Island, Hong Kong, and Calcutta. Figure 1 is a contour diagram of percentage occurrence of 1.54 GHz scintillations >15 dB observed at Ascension Island over a 3-year period taken from Mullen et al. (1984). Figure 2 is a similar contour diagram of occurrence of 3.95 GHz scintillations >2 dB observed at Hong Kong as reported by Fang and Liu (1983). Figure 3, on the other hand, shows 1.54 GHz scintillation ≥3 dB at Huancayo located near the magnetic equator (DasGupta et al., 1982). All of the above occurrence diagrams were obtained near the maximum of the current sunspot cycle. Comparison of Figures 1 and 3 shows that for the vernal equinox of 1980 (the only common data period) both stations observe 40% occurrence. However, the two magnitude levels are 15 dB and 3 dB which using Whitney (1974) and considering highly elongated rod-like irregularity anisotropy and the fact that the Huancayo measurements are made at a low elevation angle translates

to at least a 5:1 variation in integrated electron density deviation (ΔN). The recent 1.5 GHz GPS observations made from Ascension Island shown in Figure 4 provide further support to the generally assumed rod-like nature of the field-aligned irregularities in the entire equatorial belt. In addition, in-situ data shows that irregularity amplitudes (i.e., $\Delta N/N$) remain similar over the equatorial region. Thus the 5:1 ratio in integrated ΔN translates to a similar ratio in the ambient density N between the anomaly crests and the equator, at least under equinoctial conditions during solar maximum periods.

The large GHz scintillation events are all bubble related and occur in association with limited regions of total electron content (TEC) depletions. At such times TEC measurements are often not possible because of loss of correlation between the ordinary and extraordinary modes of polarization at 137 MHz (Lee et al., 1982). The TEC depletions in the anomaly regions in the sunspot maximum periods have been found to be superimposed on general post sunset TEC enhancements. These enhancements have recently been modelled by Anderson and Klobuchar (1983) on the basis of enhanced post sunset upward $\vec{E} \times \vec{B}$ drifts as observed at Jicamarca during solar maximum periods (Fejer et al., 1979) and the prevailing meridional and zonal winds. Indeed Anderson and Klobuchar (1983) have shown that the largest density at the post-sunset anomaly crests could exceed 4×10^6 m^{-3} which correspond to a critical frequency of

18 MHz. Equatorial densities at this time, on the other hand, rarely exceed 10^6 m^{-3} as observed from satellite and Plumex and Condor measurements (S. Basu et al., 1980; Szuszczewicz et al., 1980; Labelle et al., 1984). Thus a factor of 4 density enhancement is routinely observed at sunspot maximum and goes a long way in explaining the greater scintillation magnitude observed at the anomaly crests.

Another study by DasGupta et al. (1983a) has shown that there is a great variation in the magnitude of the post sunset equinoctial TEC enhancement with location within the equatorial belt. For instance, Figure 5 shows that for stations near the crest of the anomaly, Ascension Island which has large westward declination has a much larger TEC enhancement than does *Calcutta or Lunping* which have small eastward declinations. Further, the near-equatorial station, Arequipa has an ambient TEC level at 2200 LT which is much less than that observed at the crest locations. This latitude variation of TEC in the equatorial belt and its dependence on longitude during the post-sunset period can now be ordered in terms of the F-region dynamics discussed in the previous paragraph. The magnitude of equatorial scintillations is expected to follow the pattern of the TEC variation if the integrated electron density deviation controlling scintillations can be considered directly proportional to TEC. The new insight in this field is that equatorial F-region dynamics, by modulating the post-sunset background density, ultimately controls the magnitude of scintillations.

So far we have been considering primarily the

equinoctial behavior of scintillations at equatorial and crest locations and trying to provide an explanation for the greater magnitude of scintillations at the crest locations on the basis of both modelled and observed TEC behavior. If we now turn our attention to solstitial behavior of GHz scintillations we find that Ascension Island (Mullen et al., 1984) and Huancayo (Su. Basu et al., 1980) scintillations show significant GHz activity in the Decmeber solstice and not in the June solstice. The solstitial occurrence pattern is reversed when one considers 1.5 GHz activity in the Hong Kong sector (Fang and Liu, 1983). It is thus important to note that bubble-type irregularities do occur during solstices (Weber et al., 1982; Basu et al., 1983), *preferentially* at one of the two solstices depending on the longitude sector, providing a secondary maximum in scintillation activity.

Scintillation morphology can be considerably different if measurements are made at VHF frequencies like 137 and 250 MHz. In such cases, particularly in the December solstice, it is possible to observe uninterrupted patches of scintillation of 5-6 hours duration which are not associated with TEC depletions. In fact these long patches of scintillations are so numerous in the Huancayo sector that one gets a single overall maximum in scintillation occurrence in the December solstice at VHF rather than the two equinoctial maxima that appear at GHz frequencies (DasGupta et al., 1983b, cf. their Figure 1). It has been established

(Basu et al., 1984a) that these scintillation patches are due to bottomside sinusoidal (BSS) irregularities discussed at length by Valladares et al. (1983) and, as a rule, they do not give rise to GHz scintillations. Ionograms at such times show frequency spread rather than range spread which is associated with bubble type irregularities. The unique feature of the scintillation characteristics associated with BSS irregularities is the existence of Fresnel oscillations in the intensity spectra (Singleton, 1970) as shown in Figure 6 for data from Huancayo, Peru. The first seven Fresnel minima are clearly identifiable and follow the relationship $f_1 : \sqrt{2f_1} : \ldots \sqrt{nf_1}$ where f_1 = 0.2 Hz. Because of the existence of these clear minima, it is also possible to determine the ionospheric drift, v, perpendicular to the ray path by using the relationship $v/\sqrt{\lambda z} = f_1$ where λ is the radio wavelength and z the slant distance between the mean height of the irregularities and the observer. The drift in this particular case is 180 m s^{-1} which, though somewhat higher than the average, is quite consistent with zonal irregularity drifts measured by the spaced receiver drift technique in the presence of bubble-type irregularities (Basu and Whitney, 1982). Certain problems remain in regard to modeling scintillations on the basis of the in-situ structure of the BSS irregularities and these will be discussed in Section 4. The overall impact of the BSS irregularities is that scintillation morphology at a particular station becomes dependent on the frequency of observation.

related to F-region irregularities, is the signature in VHF scintillation spectra of large scale ($\sim$ several hundred meters) coherent waves in the electrojet region during both daytime and nighttime conditions (Basu et al., 1984b). The magnitude of the scintillations is quite small ($S_4 \sim 0.2$ at 137 MHz) but the manifestation of these large scale waves has important implications for the theory of electrojet irregularities (Sudan, 1983). In regard to F-region irregularities, co-ordinated radar and spaced-receiver scintillation drift experiments established for the first time that large scale irregularities ($\sim$ several hundred m) and the 3-m irregularities near the peak of the F-region travel with approximately the same speed in the E-W direction (Fejer et al., 1984). Finally, the common volume radar backscatter and 1.7 GHz scintillation measurements during the Project Condor demonstrated the simultaneous evolution of 3-m and several hundred meter scale irregularities in the onset phase and established the mutual consistency of GHz scintillation magnitudes with the rocket measurements of the background ionosphere and their structures.

the problems associated with phase and amplitude scintillation modelling.

The greatest challenge remaining in the field, other than a better elucidation of the morphology under both magnetically quiet and disturbed conditions, is the day-to-day variation of irregularity occurrence which can cause intense GHz scintillation one day, followed by an extremely calm day even under the same magnetic conditions. Our inability to predict this day-to-day variability became very apparent during the Project Condor rocket campaign when radar data of electrojet reversal at Jicamarca and magnetic field observations at Huancayo proved inadequate for predicting bubble generation later in the evening. However given the Maruyama and Matuura (1984) hypothesis discussed in Section 1, it should be interesting to be able to measure the zonal and meridional components of the neutral wind to determine whether the resultant wind vector is indeed perpendicular to the magnetic meridian on days when irregularities are observed. This could be done, for instance, by J.W. Meriwether and his colleagues at Arequipa in conjunction with Jicamarca radar and/or Huancayo/Ancon scintillation measurements. Earlier measurements of the total wind vector at Kwajalein had shown great day-to-day variability (Sipler and Biondi, 1978).

We shall conclude this review by mentioning briefly the important new results that were obtained during the Project Condor rocket campaign. A new result, which is however not

v) SUMMARY INCLUDING PROJECT CONDOR RESULTS

Considerable progress on several fronts in the equatorial scintillation field have occurred since ISEA-6. The latitude variation with greater scintillation magnitude at equatorial anomaly crests as compared to stations on the magnetic equator has been interpreted in terms of the effect of the background ambient ionization particularly during sunspot maximum conditions. Several promising leads have emerged for the resolution of the longitude variation enigma. These include the geometry of the solar terminator in relation to the magnetic meridian as well as the orientation of the thermospheric neutral wind vector with respect to the magnetic meridian as a function of longitude. Thus it has become evident that large scale F-region and, possibly also thermospheric dynamics ultimately controls the occurrence and magnitude of the observed scintillations.

A distinct category of irregularities called bottomside sinusoidal or BSS irregularities has been documented with in-situ spectra which are very different from those associated with equatorial bubbles. BSS irregularities are associated with frequency spread on ionograms and give rise to moderate levels of scintillation. The bubbles are found to give rise to the most intense scintillation events and have a two-component irregularity spectrum in both vertical and horizontal directions as measured by rockets and satellites. The observation of the two-component spectrum in the horizontal wavenumber has gone a long way in resolving many of

frequency roll-off with a spectral index on the order of p=-3 whereas the in-situ data obtained at one altitude and shown in Section 3 would indicate the expected p to be on the order of -6. While the presence of Fresnel oscillations in the scintillation spectra imply that a relatively thin layer of approximately 50 km thickness cause the scintillations, the disagreement in spectral roll-off would tend to indicate that the characteristic scale varies as a function of altitude. More studies of simultaneous in-situ BSS and scintillation spectra are needed to resolve this discrepancy.

one-dimensional power law index exceeding -2. The emergence of focusing in saturated VHF scintillations provides information on irregularity scales larger than the Fresnel scale (Vats et al., 1981) and the absence of S_4 far above unity is caused by shallow slopes at large irregularity scales. Almost all these features in the modelled spectra are actually observed in the very strong irregularity environment at Ascension Island. Modelling of both phase and intensity scintillations for the case of single and two-component irregularity spectrum has been undertaken by Rino and Owen (1984). These authors considered a phase power spectrum equivalent to an irregularity spectrum with an index of 1 at the large scale end and an index of 3 in the small scale length range with variable values of break scale length ($2\pi/k_b$) at which transition of the spectral indices occur. They computed numerically the phase spectra obtained at various distances (z_p) from the phase screen having phase realizations corresponding to a strength of turbulence $C_s = 10^{22}$ and break scale lengths of 500 m and 1 km. Figures 14(a) and 14(b) illustrate the interesting results indicating that at short break scale lengths the phase spectral slope becomes shallower than the in-situ spectrum because of cycle slips (i.e., large near discontinuous phase changes) at much smaller distances from the phase screen.

Modelling of scintillations arising from BSS irregularities has not yet been undertaken. However, as discussed in Section 1, scintillation spectral observations show a high

iv) SCINTILLATION MODELLING

In light of the in-situ measurements discussed above, it is important to determine whether the radio scintillation data, which are sensitive to the electron density perturbation integrated over the whole propagation path, are consistent with the multiple component power-law spectrum or the sinusoidal spectrum under weak as well as strong scatter conditions.

Such a study for intensity scintillations associated with bubbles was performed by Franke and Liu (1983) who used the horizontal in-situ irregularity structure determined by Basu et al. (1983) to model the observed scintillations. Their modelled spectra are shown in Figure 13 for the VHF, L and C-band signals in the case of a two-component irregularity power spectrum. The integrated electron density deviation was such that the C-band signals suffered weak scattering, the L-band signals encountered strong scattering and the VHF signals were driven far into saturation. The steep high frequency slope of the C-band spectrum in Figure 13 is consistent with the assumed one-dimensional in-situ irregularity spectrum with a slope of -3.5 for the small scale regime. The L-band spectrum shows first a slope of -6.5 and then a tail that approaches the slope of the C-band spectrum. The VHF spectrum shows an extended flat low-frequency portion and a steep high frequency slope. The steepening of the spectral slopes for strong scattering was modelled by Rino (1980) and Booker and MajidiAhi (1981) for single component power law spectrum with

the spectral index was found to decrease systematically with increasing perturbation strength. The shallowing of the spectral slope at the long scalelength range has important ramifications for phase and amplitude scintillation modelling which we shall discuss in Section 4.

The in-situ structure of the BSS irregularities is quite different from those associated with bubbles. Figure 12 (bottom panel) shows one frame of high resolution AE-E data taken at approximately the time when the scintillations shown in Figure 6 were observed (Basu et al., 1984a). The density data (solid line) shows a quasi-sinusoidal structure and the pitch (i.e., vertical drifts shown as a series of dots) shows mostly an anti-correlation with the density structure as was also noted by Valladares et al. (1983). The spectrum on the top panel is for the detrended data shown below with the crosses showing the Fourier (FFT) spectrum and the solid line the maximum entropy (MEM) spectrum. We find that the roll-off on the high frequency part between irregularity scalelengths of 1 km and 200 m is very steep, the one-dimensional index being -5.37. The low frequency portion also shows a gentle roll-off with the peak power being at 1 km. The irregularity amplitude is 3.5 percent and the background density is almost 10^5 cm^{-3}. The spectrum is thus of the gaussian form and not at all similar to the multi-component power-law that is associated with equatorial bubbles and shown in Figure 11.

iii) IRREGULARITY STRUCTURE

In-situ probing of F-region irregularities has been very important in understanding the nature of equatorial irregularities causing scintillations. We only discuss here the findings that are of the greatest use in scintillation modelling. The recent in-situ measurements of the one-dimensional vertical and horizontal (magnetic E-W) spatial power spectrum of the ionospheric irregularities that occur within equatorial bubbles have shown that the spectra often exhibit a pronounced break in their power-law behavior at a spatial scale in the range 500 m - 1 km (Rino et al., 1981; Kelley et al., 1982; Basu et al., 1983). One of the 2 Condor F-region rocket data also shows a similar break in the slope (LaBelle et al., 1984). The Plumex rocket results of the vertical wave number spectrum is shown in Figure 10 and the horizontal wave number spectrum (more relevant for scintillation modelling) derived from AE-E by Basu et al. (1983) is shown in Figure 11. The measurements reported by Basu et al. (1983) for the horizontal spectra indicate that when the break is present, the power law index of the one-dimensional spectra in the large scale length regime p_ℓ is between -1 and -1.5 while the spectral index in the short scalelength range p_s is between -3 and -3.5. These measurements are consistent with earlier results reported by Livingston et al. (1981), also from AE-E data obtained at another longitude sector, for the kilometer and larger scale regime which showed an average spectral index $p_\ell \sim -1.8$. In the Livingston et al. study,

However, while the former requires the magnetic flux tube to move into sunset conditions simultaneously thereby generating the largest longitudinal gradients of integrated Pederson conductivity, the latter requires the height at both ends of the flux tube to remain the same resulting in a symmetric electron density distribution about the magnetic equator. A complete explanation of the longitudinal variation probably will require elements of both hypotheses. In order that careful comparisons of predictions and scintillation data can be made on the seasonal-cum-longitudinal behavior, we provide in Figure 9 a synoptic morphology of scintillation occurrence as a function of longitude obtained by putting together observations from many of the stations marked on the map. The periods of *maximum* scintillation activity (E for equinoxes and D and J for the December and June solstices, respectively) as a function of longitude are indicated where observations exist. We find that a change over in solstitial behavior occurs somewhere over the Pacific (where there are no observations over a 90° longitude sector) and another occurs rather abruptly between 90°E to 120°E in Asia. We would like to urge that scintillation measurements be made either from Christmas Island (CI on Figure 9) or Tahiti (TA) to bridge the huge gap in our observations and provide uniform coverage against which predictions can be tested. It is hoped that a synthesis of the ideas discussed above will provide a complete explanation of the longitudinal control of equatorial scintillations.

northern winter in the region of large westward declination (at the Atlantic longitudes), and during the northern summer in the region of large eastward declination (at the Pacific longitudes). Thus the authors conclude that the absence of a transequatorial component of the thermospheric wind which produces symmetric density distribution helps in the growth of the Rayleigh Taylor instability. This is because the presence of a meridional component of the wind raises the F-region at one end of the magnetic flux tube and lowers it in its conjugate hemisphere thus altering the loss rate of the plasma within the tube and enhancing its integrated Pederson conductivity by the larger contribution from the low altitude end. We know from the modelling work of Anderson and Haerendel (1979) and Zalesak et al. (1982) and the scintillation and radar observations of Weber et al. (1983) and Tsunoda (1980) that the entire flux tube takes part in the instability process, so that it is the integrated Pederson conductivity that controls the growth rate of the instability. It is necessary to note, however, that careful modelling studies are needed to verify whether the integrated loss rate is indeed greater than the growth rate of the Rayleigh-Taylor instability under the conditions envisaged by Maruyama and Matuura (D.N. Anderson, private communication, 1984).

Thus we find that both the Tsunoda hypothesis and that by Maruyama and Matuura depend on the varying declination of the earth's magnetic field as a function of longitude.

solstice. A clear systematic variation in the shape of the magnetic meridional distributions of the electron density can be seen depending both upon the longitude of observation and time of year. The electron density distribution was found to be symmetric about the magnetic equator both at the Atlantic longitude in the northern winter period and at the Pacific longitude in the northern summer. During these periods Maruyama and Matuura (1984) found an enhancement in spread F activity and the occurrence of bubbles in their topside data. Conversely, the electron density distribution was found to be asymmetric both at the Atlantic longitude in the northern summer and at the Pacific longitude in the December months when the spread-F activity was found to be quite low. On the basis of these ISS-b observations, the authors suggest that possibly a transequatorial component of the thermospheric neutral wind, which creates the asymmetric density distribution, suppresses the growth of the Rayleigh Taylor instability which is widely accepted as responsible for equatorial bubbles (Ossakow, 1981). We note that, in general, the thermospheric neutral winds in the F region tend to blow from the diurnal pressure bulge around 15 hours LST at the sub-solar latitude towards the antipode of the bulge (Rishbeth, 1972). Therefore, the direction of the thermospheric neutral wind in the nighttime equatorial regions tends to be perpendicular to the magnetic meridian during the equinoxes in the region of small declination angle of the magnetic field (at the Indian longitudes), during the

in the December solstice. Indeed, 2½ years of data taken at Natal at 250 MHz showed a single maximum in the November-December months (Yeh et al., 1981). However, the problem with the Tsunoda hypothesis is that it does not predict the secondary maximum at many longitudes. The much studied Huancayo sector is a case in point. There the two solstices behave very differently in terms of scintillation activity with the December occurrence far exceeding the June levels (Aarons, 1982 and references therein). However, the predicted activity is centered almost exactly on the equinoxes with nothing to indicate the asymmetric behavior at the 2 solstices. Thus, while the Tsunoda hypothesis provides some ordering in a chaotic situation, a great deal of scintillations does occur (even at GHz which are bubble-related but more widely in the 137-250 MHz range which are probably BSS-related) at times when the geomagnetic flux tubes do not align with the solar terminator.

Another recent paper, that by Maruyama and Matuura (1984), addresses the question of the solstitial behavior of equatorial irregularities at different longitudes. Figure 8 shows mean electron density distributions along the magnetic meridians at the Japanese topside sounder satellite ISS-b altitude of 1100 km at two typical longitudes, 30°W (Atlantic) and 150°W (Pacific). This is derived from the global density distribution maps for two periods, namely October 1979 to February 1980 to represent the northern winter solstice and April to August, 1980 to represent the northern summer

ii) LONGITUDE VARIATION

The longitudinal variation of equatorial irregularities during a solstice became quite vividly evident on the basis of in-situ data and provided a framework for the interpretation of scintillation observations from far flung stations (Basu et al., 1976). Since then, GHz measurements, some of them discussed in the last section, have shown that in general the primary maxima are seen near the equinoxes at most longitudes, whereas the solstitial behavior is a function of longitude. Recently, Tsunoda (1984) advanced the hypothesis that scintillation-producing irregularities are most likely to develop in the equatorial F-layer when the integrated E-region Pedersen conductivity experiences its maximum longitudinal gradient. Based on this postulate, Tsunoda predicted that scintillation activity would maximize at a given longitude at times of year when the solar terminator is most nearly aligned with the geomagnetic flux tubes in that sector. Secan and Fremouw (1983) used Tsunoda's prediction to model the seasonal cum longitudinal behavior of equatorial irregularity strength, $C_S L$, where C_S is the strength of turbulence (Rino, 1979) and L the irregularity layer thickness, at four stations at 2230 LT for high sunspot conditions and the modelled values are shown in Figure 7. From Figure 7, we may note that while maxima in irregularity occurrence are predicted near the equinoxes at Huancayo, Kwajalein and Guam, at Natal the maxima appear

The dependence of this morphology on sunspot cycle is important if a station is off the equator as the variation of the irregularity belt width can bring the station either into the belt as the altitude of the F-region irregularities increases at the equator and maps to a wider region or out of it in the decreasing phase (Basu and Basu, 1983). Based on the scintillation measurements made simultaneously at four stations with different latitudes in the equatorial region, during the sunspot maximum period, Somayajulu et al. (1984) have established the coupling between the equator and stations away from it. This feature as a function of solar cycle was quite convincingly demonstrated by DasGupta et al. (1981) who showed that the scintillation occurrence at Calcutta during the two equinoxes and the December solstice increased as a function of solar cycle while scintillation occurrence during the June solstice, probably of local origin, remained independent of solar activity. Thus occurrence of scintillations during different seasons at the same station may vary considerably depending on the sunspot cycle. There is evidence that beyond the anomaly crest the scintillations fall off extremely rapidly with increasing latitude (Wernik et al., 1983).

ACKNOWLEDGMENTS

We thank many of our colleagues who made their diagrams available to us in advance of publications. We appreciate the efforts of E. MacKenzie in the preparation of the manuscript. The work at Emmanuel College was supported by AFGL Contracts F19628-81-K-0011 and F19628-84-K-0003.

REFERENCES

AARONS J.	1977	IEEE Trans. Antennas Propagat., AP-25, 729.
AARONS J.	1982	Proc. IEEE, 70, 360.
AARONS J., WHITNEY H.E., MACKENZIE E. and BASU S.	1981	Radio Sci., 16, 939.
AARONS J., KLOBUCHAR J.A., WHITNEY H.E., AUSTEN J., JOHNSON A.L. and RINO C.L.	1983	Radio Sci., 18, 421.
ANDERSON D.N. and HAERENDEL G.	1979	J. geophys. Res., 84, 4251.
ANDERSON D.N. and KLOBUCHAR J.A.	1983	J. geophys. Res., 88, 8020.
BASU S. and BASU Su.	1981	J. atmos. terr. Phys., 43, 473.
BASU S. and WHITNEY H.E.	1983	Radio Sci., 18, 263.
BASU S., MCCLURE J.P., BASU Su., HANSON W.B. and AARONS J.	1980	J. geophys. Res., 83, 5119.
BASU S., BASU Su., VALLADARES C.E., MCCLURE J.P., DASGUPTA A. and WHITNEY H.E.	1984a	To be submitted to Geophys. res. Lett.
BASU S., BASU Su., KELLEY M.C., PFAFF R., KUDEKI E. and BAKER K.D.	1984b	To be submitted to J. geophys. Res.
BASU S., BASU Su., LABELLE J., KUDEKI E., FEJER B.G., KELLEY M.C. and WHITNEY H.E.	1984c	To be submitted to J. geophys. Res.
BASU Su. and KELLEY M.C.	1977	J. atmos. terr. Phys., 39, 1229.
BASU Su. and KELLEY M.C.	1979	Radio Sci., 14, 471.
BASU Su., BASU S. and KHAN B.K.	1976	Radio Sci., 11, 821.
BASU Su., BASU S., MULLEN J.P. and BUSHBY A.	1980	Geophys. res. Lett., 7, 259.

BASU Su., BASU S., MCCLURE J.P., HANSON W.B. and WHITNEY H.E.	1983	J. geophys. Res., 88, 403.
BOOKER H.G. and MAJIDIAHI G.	1981	J. atmos. terr. Phys., 43, 1199.
DASGUPTA A., MAITRA A. and BASU S.	1981	Radio Sci., 16, 1455.
DASGUPTA A., AARONS A. KLOBUCHAR J.A., BASU S., and BUSHBY A.	1982	Geophys. res. Lett., 9, 147.
DASGUPTA A., BASU S., AARONS J., KLOBUCHAR J.A., BASU Su., and BUSHBY A.	1983a	J. atmos. terr. Phys., 45, 15.
DASGUPTA A., ANDERSON D.A., and KLOBUCHAR J.	1983b	Adv. space Res., 2, 199.
FANG D.J. and LIU C.H.	1983	Radio Sci., 18, 241.
FARLEY D.T.	1974	Rev. Geophys. space Phys., 12, 285.
FEJER B.G. and KELLEY M.C.	1980	Rev. Geophys. space Phys., 18, 401.
FEJER B.G., FARLEY D.T., WOODMAN R.F. and CALDERON C.	1979	J. geophys. Res., 84, 5792.
FEJER B.G., KUDEKI E., BASU S., BASU Su. and FARLEY D.T.	1984	To be submitted to J. geophys. Res.
FRANKE S.J. and LIU C.H.	1983	J. geophys. Res., 88, 7075.
KELLEY M.C. and MCCLURE J.P.	1981	J. atmos. terr. Phys., 43, 427.
KELLEY M.C., PFAFF R., BAKER K.D., ULWICK J.C., LIVINGSTON R., RINO C. and TSUNODA R.	1982	J. geophys. Res., 87, 1575.
LaBELLE J., KELLEY M.C., KINTNER P.M., PFAFF R.F., SIEFRING C., BASU S., BASU Su., BAKER K.D. and RAO N.B.	1984	To be submitted to J. geophys. Res.

LEE M.C., DASGUPTA A., KLOBUCHAR J.A., BASU S., and BASU S.	1982	Radio Sci., 17, 399.
LIVINGSTON R.C., RINO C.L., MCCLURE J.P. and HANSON W.B.	1981	J. geophys. Res., 86, 2421.
MARUYAMA T. and MATUURA N.	1984	Submitted to J. geophys. Res.
OSSAKOW S.L.	1979	Rev. Geophys. space Phys., 17, 521.
OSSAKOW S.L.	1981	J. atmos. terr. Phys., 43, 437.
RINO C.L.	1979	Radio Sci., 14, 1135.
RINO C.L.	1980	Radio Sci., 15, 41.
RINO C.L. and OWEN J.	1984	Radio Sci., 19, 891.
RINO C.L., TSUNODA R.T., PETRICEKS J., LIVINGSTON R.C., KELLEY M.C. and BAKER K.D.	1981	J. geophys. Res., 86, 2411.
RISHBETH H.	1972	J. atmos. terr. Phys., 34, 1.
SINGLETON D.G.	1970	J. atmos. terr. Phys., 36, 113.
SIPLER D.P. and BIONDI M.A.	1978	Geophys. res. Lett., 5, 373.
SOMAYAJULU Y.V., GARG S.C., DABAS R.S., SINGH L., TYAGI T.R., LOKANADHAM B., RAMAKRISHNA S. and NAVNEETH G.	1984	Radio Sci., 19, 707.
SUDAN R.N.	1983	J. geophys. Res., 88, 4853.
SZUSZCZEWICZ E.P., TSUNODA R.T., NARCISI R., and HOLMES C.	1980	Geophys. res. Lett., 7, 537.
TSUNODA R.T.	1980	J. atmos. terr. Phys., 42, 743.
TSUNODA R.T.	1984	Submitted to J. geophys. Res.

VALLADARES C.E., HANSON W.B., MCCLURE J.P. and CRAGIN B.L.	1983	J. geophys. Res., 88, 8025.
VATS H.O., BOOKER H.G. and MAJIDIAHI G.	1981	J. atmos. terr. Phys., 43, 1235.
WEBER E.J., BRINTON H.C., BUCHAU J. and MOORE J.G.	1982	J. geophys. Res., 87, 10503.
WEBER E.J., AARONS J. and JOHNSON A.L.	1983	J. geophys. Res., 88, 3175.
WERNIK A.W., FRANKE S., LIU C.H. and FANG D.J.	1983	Geophys. res. Lett., 10, 155.
YEH K.C., MULLEN J.P., MEDEIROS J.R., DASILVA R.F. and MEDEIROS R.T.	1981	J. geophys. Res., 86, 7527.
YEH K.C. and LIU C.H.	1982	Proc. IEEE, 70, 324.
ZALESAK S.T., OSSAKOW S.L. and CHATURVEDI P.K.	1982	J. geophys. Res., 87, 151.

Reference is also made to the following unpublished material:

BASU Su. and BASU S.	1983	Proceedings of International Symposium on "Beacon Satellite Studies of the Earth's Environment", New Delhi, India.
MULLEN J.P., MACKENZIE E., BASU S. and WHITNEY H.E.	1984	Proc. of IES, Alexandria VA.
SECAN J.A. and FREMOUW E.J.	1983	Progress Rpt. No. 2, Physical Dynamics, Bellevue WA.
WHITNEY H.E.	1974	Notes on the relationship of scintillation index to probability distributions and their uses for system design, AFCRL-TR-74-0004.

FIGURE CAPTIONS

Figure 1 - Contour plots of monthly mean percentage occurrence of scintillations ≥15 dB at 1.54 GHz observed at Ascension Island, 1980 - 1982 (after Mullen et al., 1984).

Figure 2 - Contour plots of monthly mean percentage occurrence of 3.95 GHz ionospheric scintillation events ≥2 dB at Hong Kong (after Fang and Liu, 1983).

Figure 3 - Contour plots of monthly mean percentage occurrence of scintillations ≥3 dB at 1.54 GHz observed at Huancayo (after DasGupta et al., 1982).

Figure 4 - Median S_4 index shown along the tracks of several GPS satellites for scintillation measurements at 1.6 GHz during 24 January - 11 February 1981. Detection of high scintillation levels at many elevations and azimuths imply absence of sheet-like irregularities aligned with the magnetic meridian (after Aarons et al., 1983).

Figure 5 - Total electron content (TEC) measurements performed at three stations near crest of the equatorial anomaly (Ascension, Lunping, and Calcutta) and one station close to the magnetic equator (Arequipa) during the two equinoxes, March (solid line) and September (dashed line). The local times are: Ascension Island (UT-1h), Calcutta (UT+6h), Lunping (UT+8h), and Arequipa (UT-5h). Note large post-sunset TEC enhancement at anomaly crest stations (after DasGupta et al., 1983b).

Figure 6 - 249 MHz scintillations from LES-8 observed at Huancayo during occurrence of bottomside sinusoidal (BSS) irregularities. Note presence of seven Fresnel minima as marked along frequency axis (after Basu et al., 1984a).

Figure 7 - Variation of modelled values of integrated strength of turbulence as a function of day of the year at four equatorial stations at different longitudes using Tsunoda's (1984) hypothesis for irregularity generation (after Secan and Fremouw, 1983).

Figure 8 - Latitudinal variation of electron density measured by topside sounder satellite ISS-b at two different longitudes during October 1979-February 1980 and April-August 1980. Note symmetry in latitudinal variation occurs at two different times at the two longitudes (after Maruyama and Matuura, 1984).

Figure 9 - Synoptic map of maximum occurrence of scintillations as a function of longitude. Note maximum occurrence of scintillations during equinoxes (E) and December solstice (D) in the ±80° longitude sector and maximum occurrence during two E months and June solstice in the 110°E to 170°W sector.

Figure 10 - Plumex rocket measured in-situ electron density irregularity spectrum at 316 km showing break near $k=2\ km^{-1}$ (after Rino et al., 1981).

Figure 11 - A 3-sec sample of high resolution RPA data of relative amplitudes (lower panel) obtained on AE-E orbit 22759 at 436 km within an equatorial bubble with its spectrum (top panel) showing a break at scalelength of 1 km (after Basu et al., 1983).

Figure 12 - A 3-sec sample of high resolution RPA data of relative amplitudes (solid line) and vertical velocity (dots) obtained on AE-E orbit 22700 at 440 km within bottomside sinusoidal (BSS) structure (lower panel) and its spectrum (top panel) showing very steep fall-off at high frequency end (after Basu et al., 1984a).

Figure 13 - Multi-frequency temporal scintillation spectra computed from simulated scintillation data for the two-component power-law irregularity spectrum model (after Franke and Liu, 1983).

Figure 14 - Phase spectra at different propagation distances for two-component power-law irregularity spectrum (after Rino and Owen, 1984).

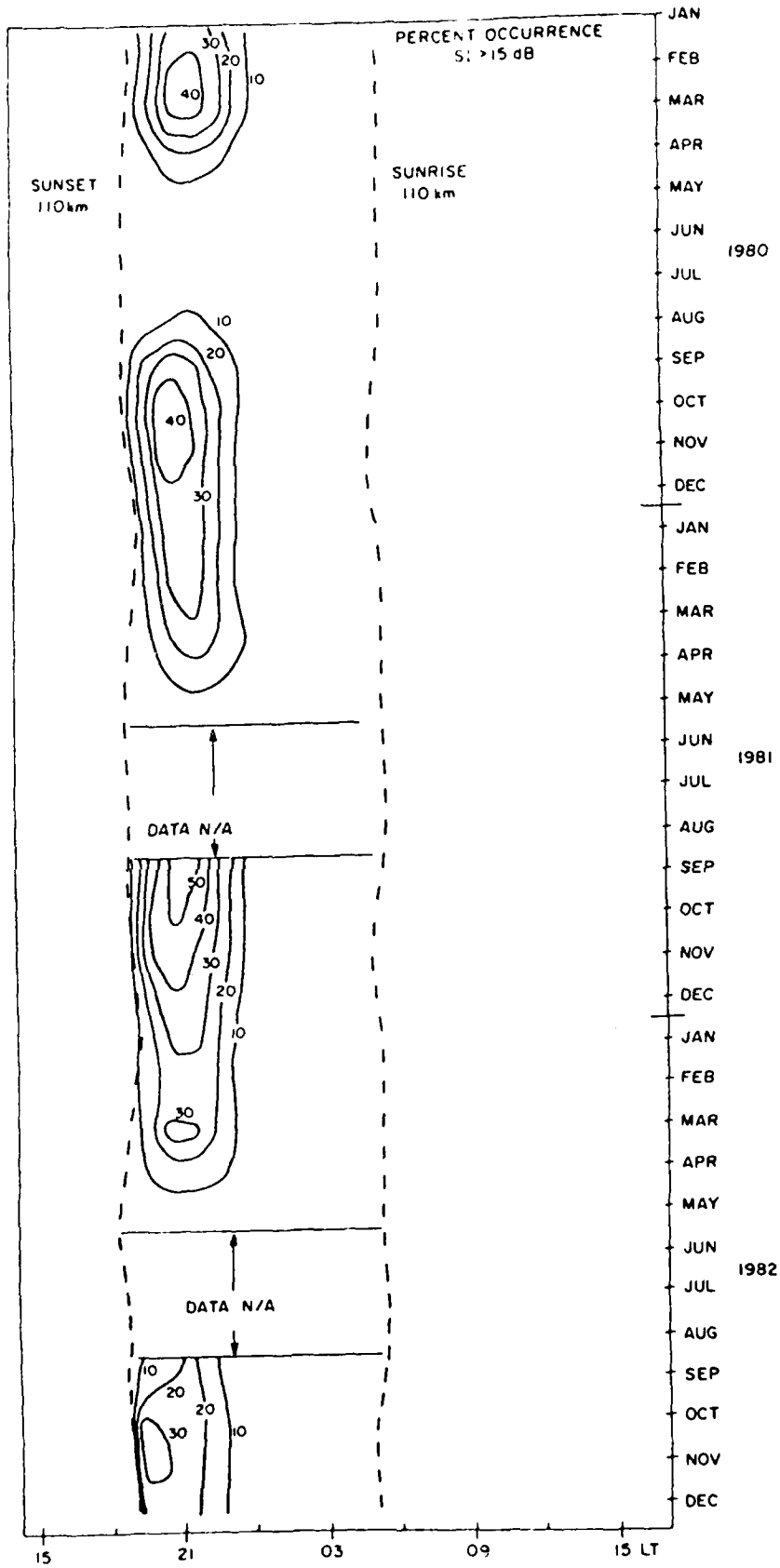

ASCENSION ISLAND ALL K MS LBD

Figure 1

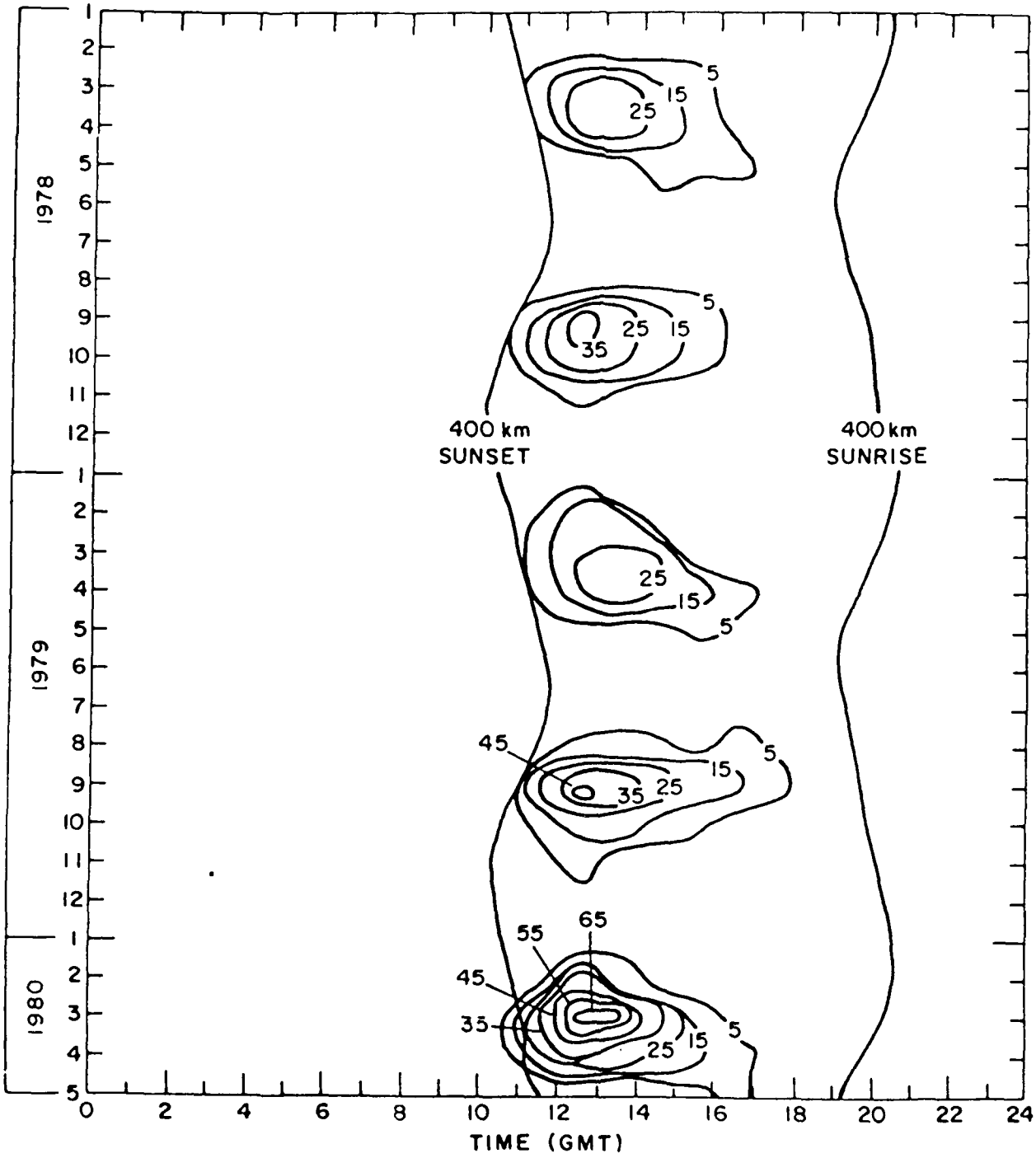

PACIFIC OCEAN SATELLITE

(Fang and Liu, "Scintillation in Asian Region", Radio Sci., 1983)

Figure 2

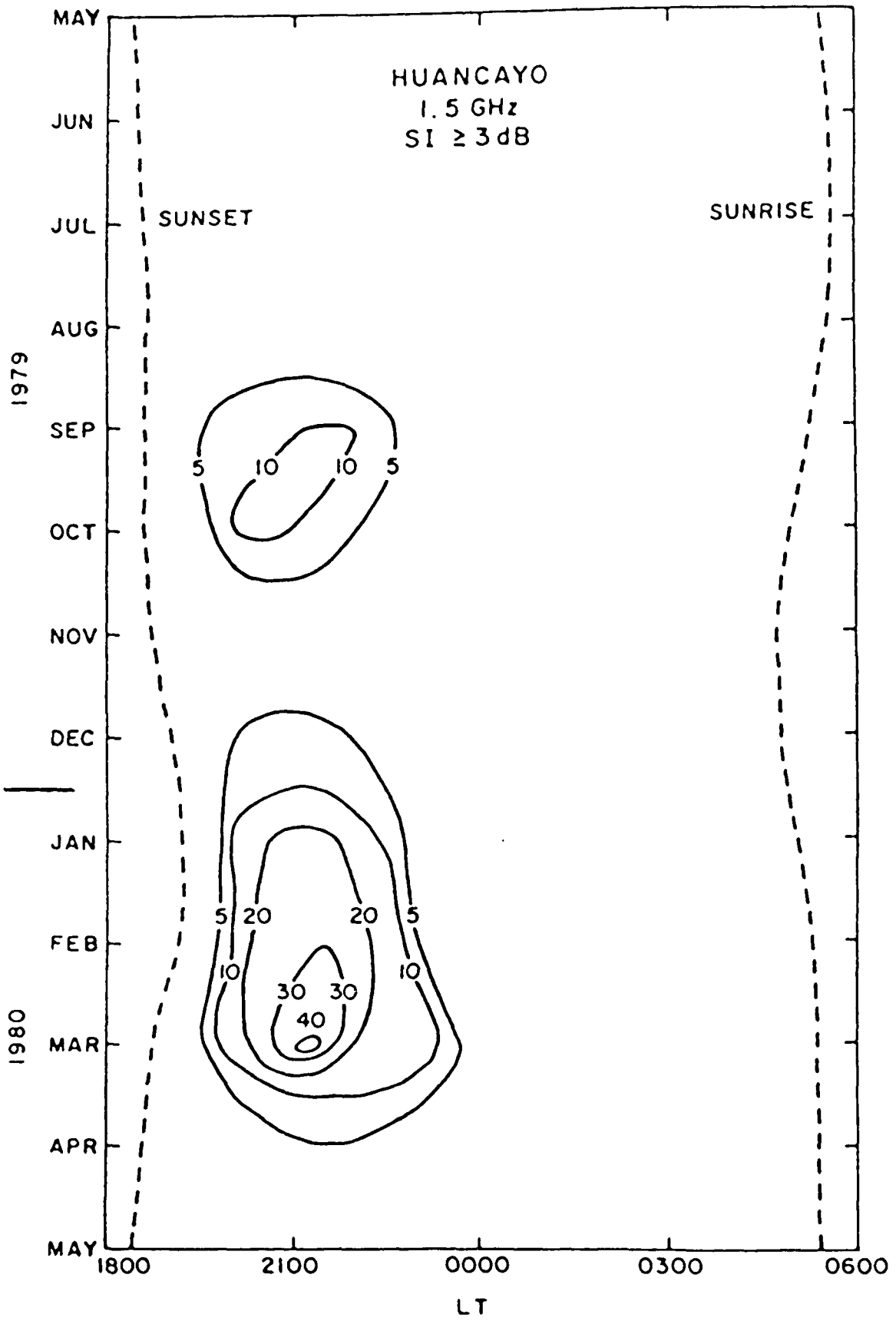
HUANCAYO
1.5 GHz
SI ≥ 3dB
SUNSET
SUNRISE
MAY
JUN
JUL
AUG
SEP
OCT
NOV
DEC
JAN
FEB
MAR
APR
MAY
1979
1980
5
10
10
5
5
20
20
5
10
10
30
30
40
1800
2100
0000
0300
0600
LT

Figure 3

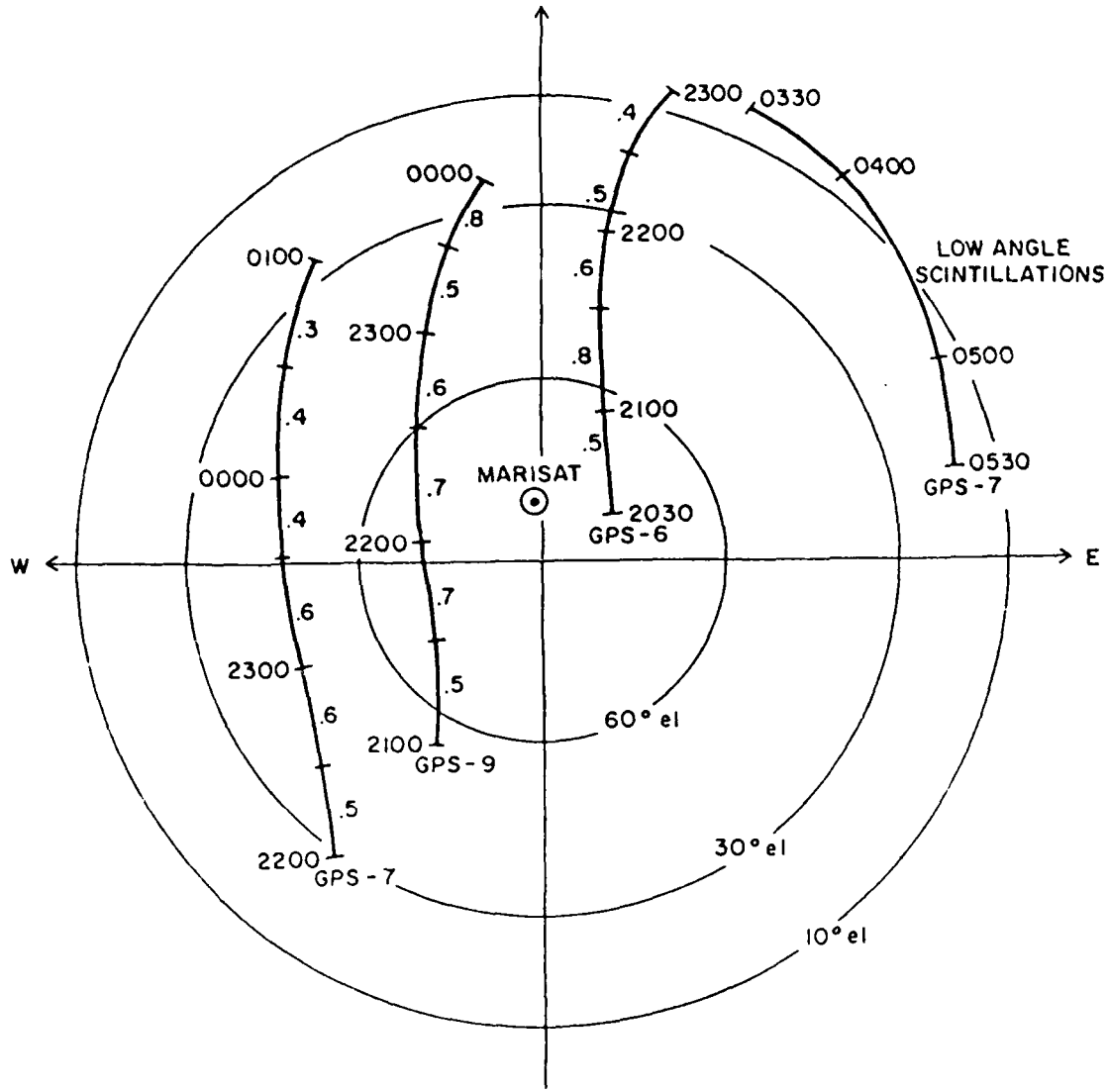

MEDIAN LEVELS OF SCINTILLATION WHEN $S_4 \geq .3$

Figure 4

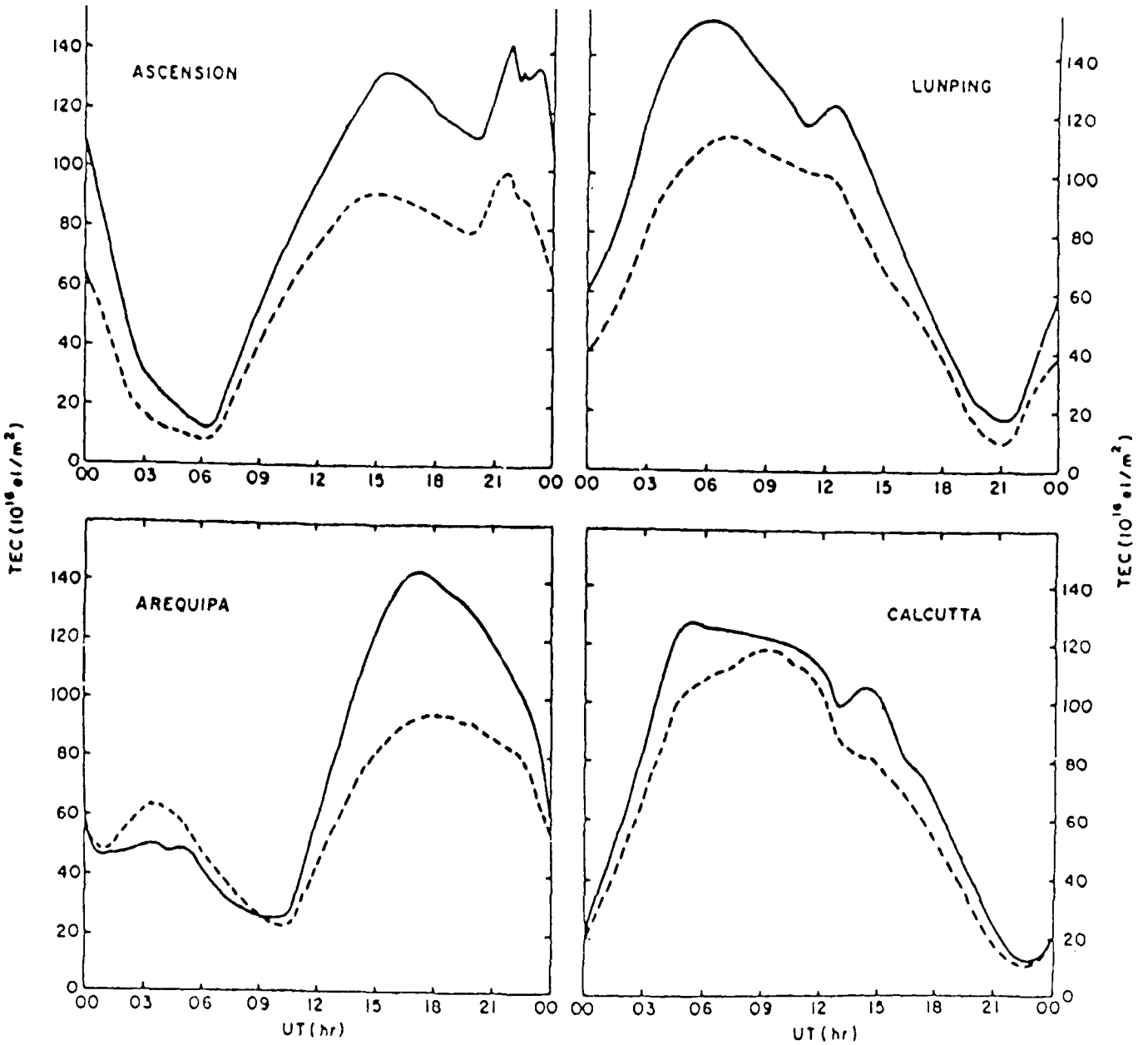
ASCENSION
LUNPING
AREQUIPA
CALCUTTA
TEC (10^{16} e1/m^2)
UT (hr)
0
20
40
60
80
100
120
140
00
03
06
09
12
15
18
21

Figure 5

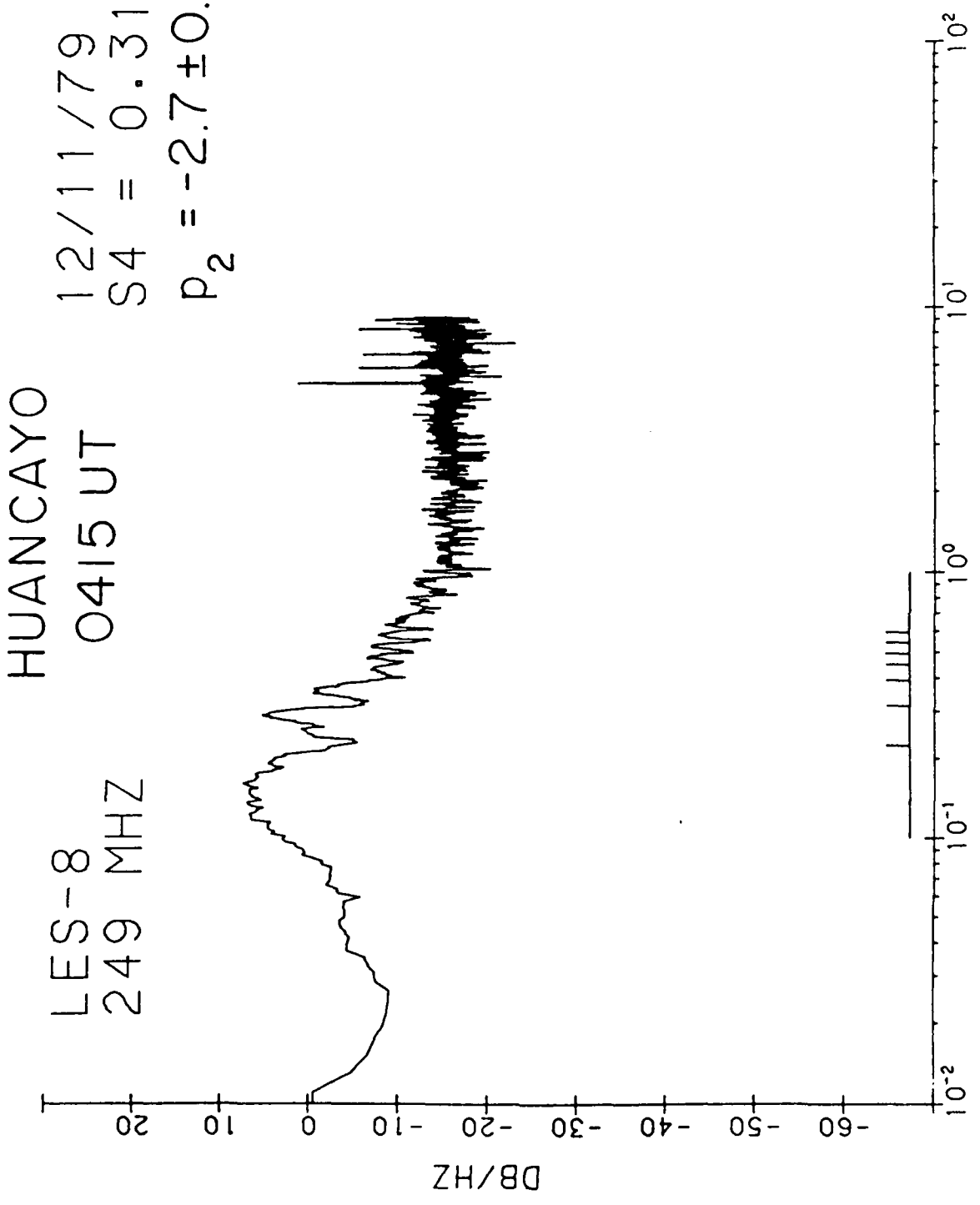
HUANCAYO
0415 UT
12/11/79
S4 = 0.31
p_2 = -2.7±0.3
LES-8
249 MHZ
DB/HZ
20
10
0
-10
-20
-30
-40
-50
-60
10^{-2}
10^{-1}
10^{0}
10^{1}
10^{2}
FREQUENCY - HZ

Figure 6

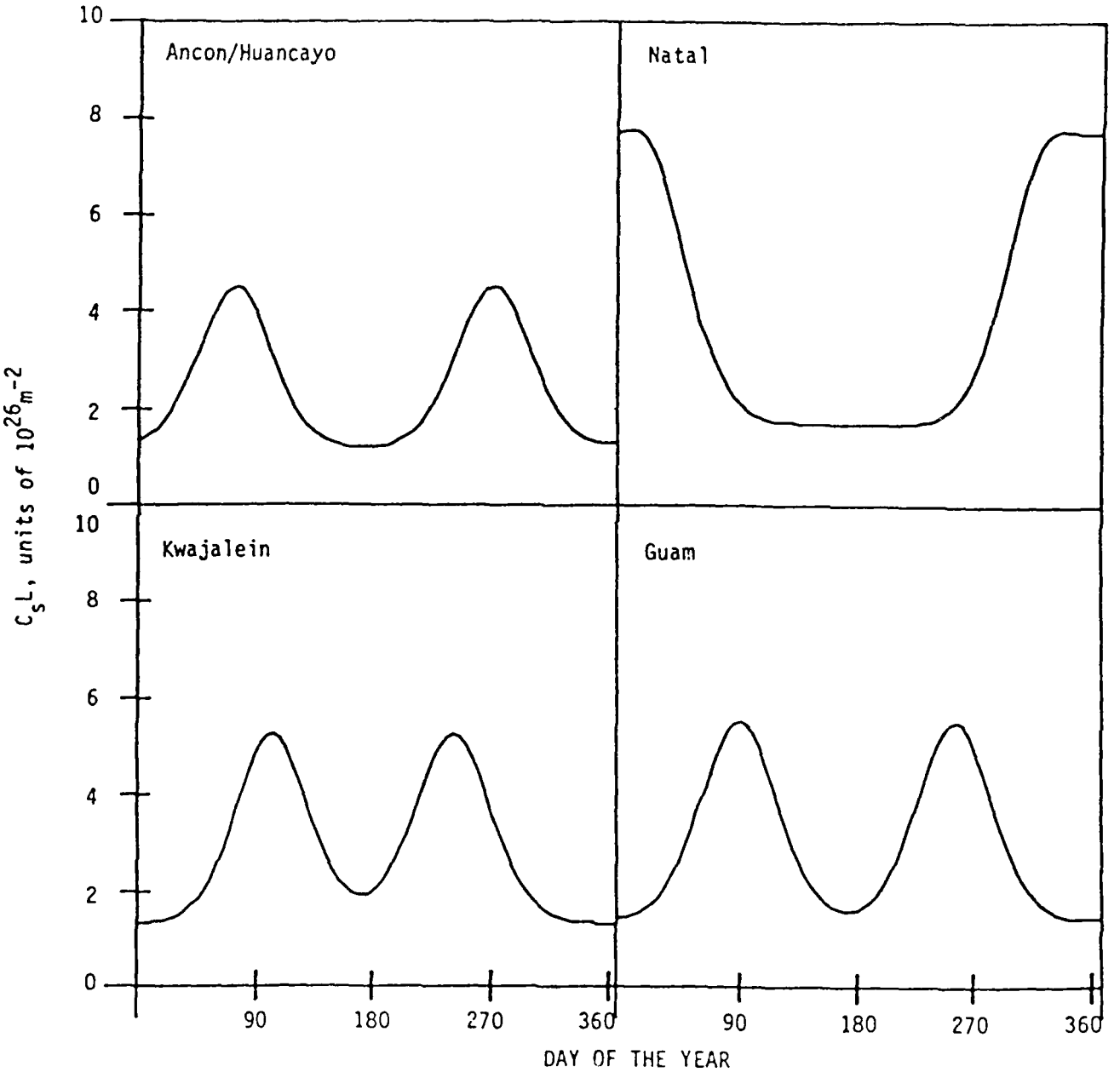
Ancon/Huancayo
Natal
Kwajalein
Guam
10
8
6
4
2
0
90
180
270
360
C_sL, units of $10^{26}m^{-2}$
DAY OF THE YEAR

Figure 7

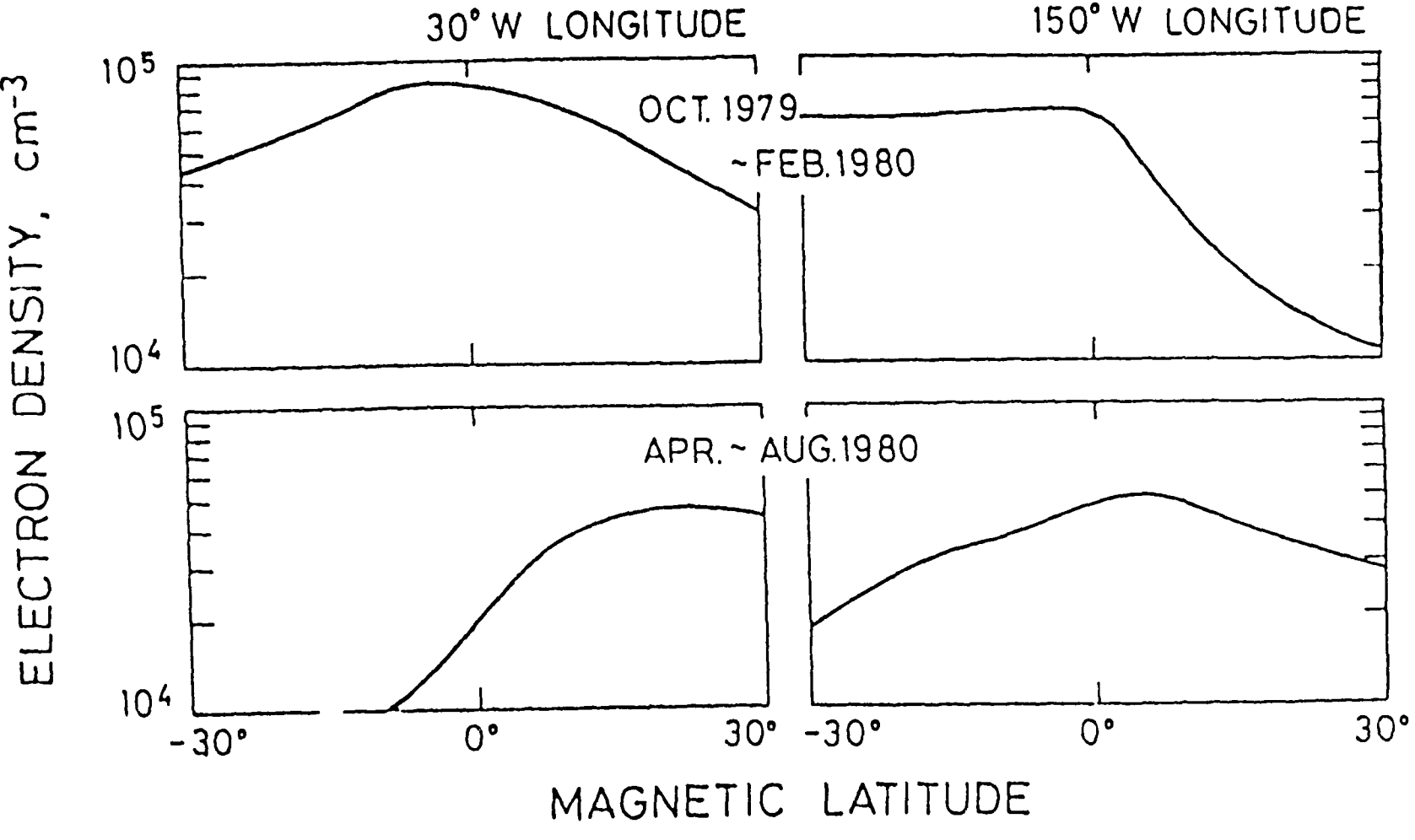
30° W LONGITUDE
150° W LONGITUDE
OCT. 1979
~FEB. 1980
APR. ~ AUG. 1980
10^5
10^4
ELECTRON DENSITY, cm^{-3}
-30°
0°
30°
MAGNETIC LATITUDE

Figure 8

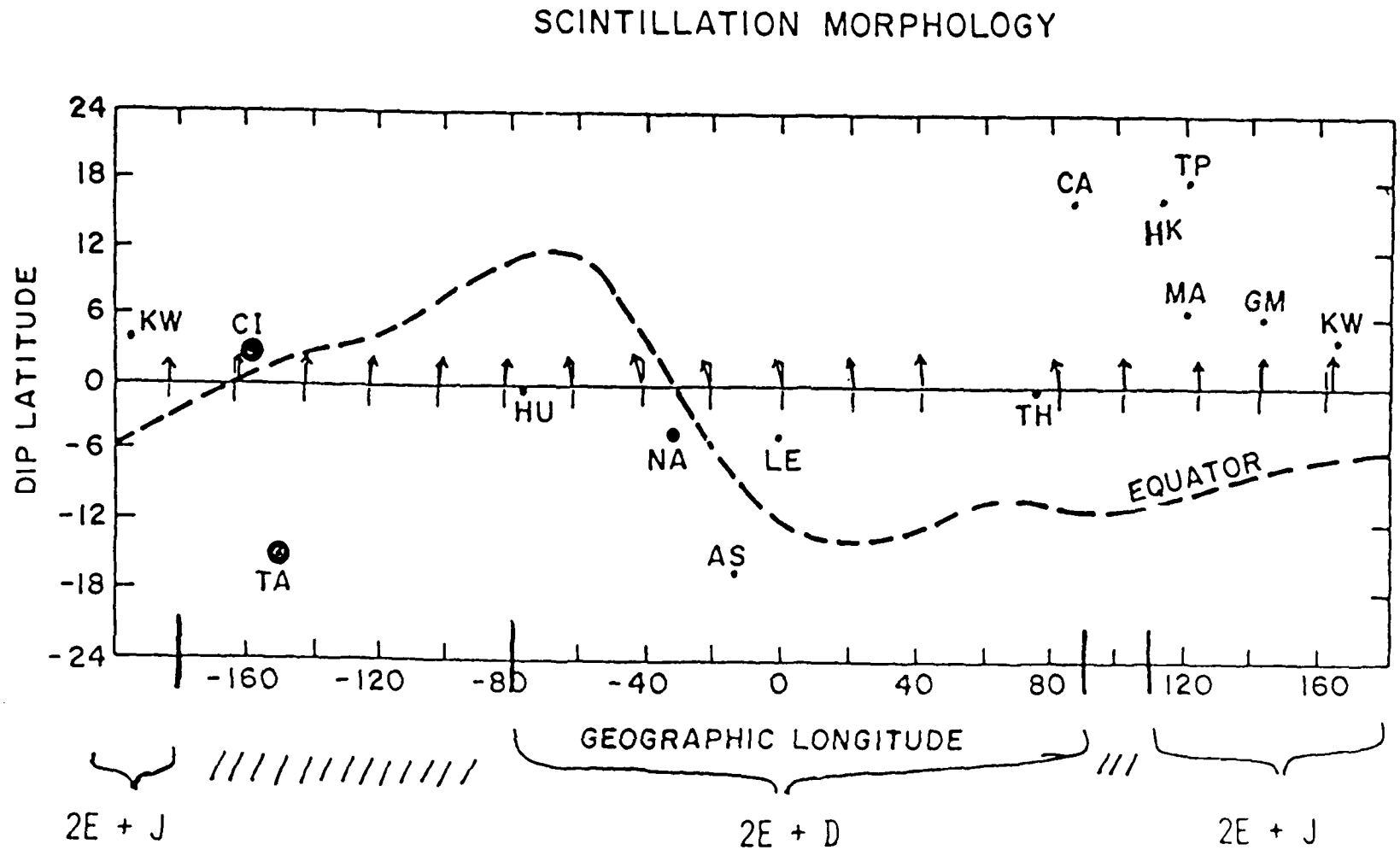
SCINTILLATION MORPHOLOGY
DIP LATITUDE
24
18
12
6
0
-6
-12
-18
-24
KW
CI
TA
HU
NA
LE
AS
TH
CA
TP
HK
MA
GM
KW
EQUATOR
-160
-120
-80
-40
0
40
80
120
160
GEOGRAPHIC LONGITUDE
2E + J
2E + D
2E + J

Figure 9

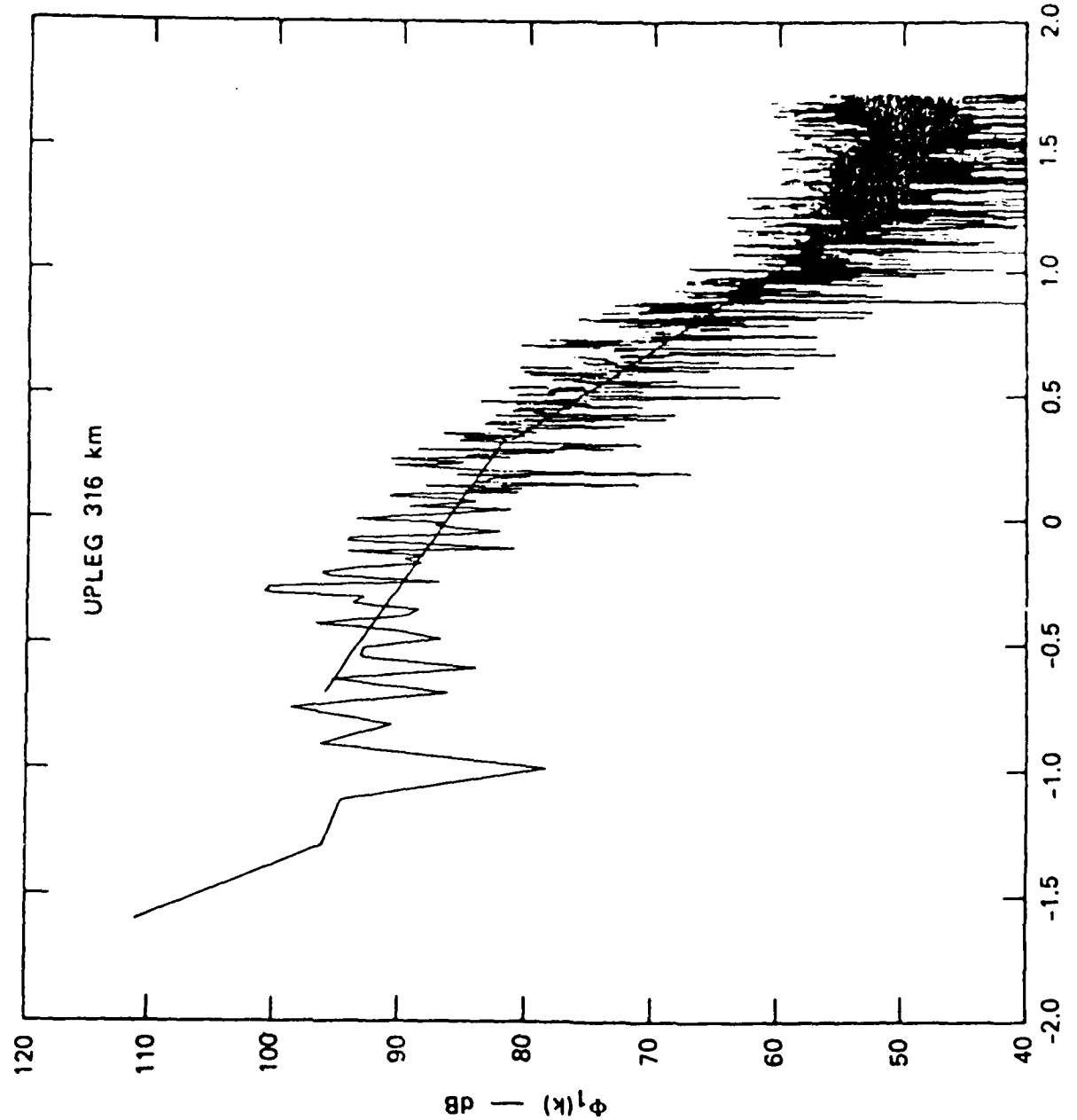
UPLEG 316 km
$\Phi_1(k)$ — dB
$\log_{10}k$ — km^{-1}
120
110
100
90
80
70
60
50
40
-2.0
-1.5
-1.0
-0.5
0
0.5
1.0
1.5
2.0

Figure 10

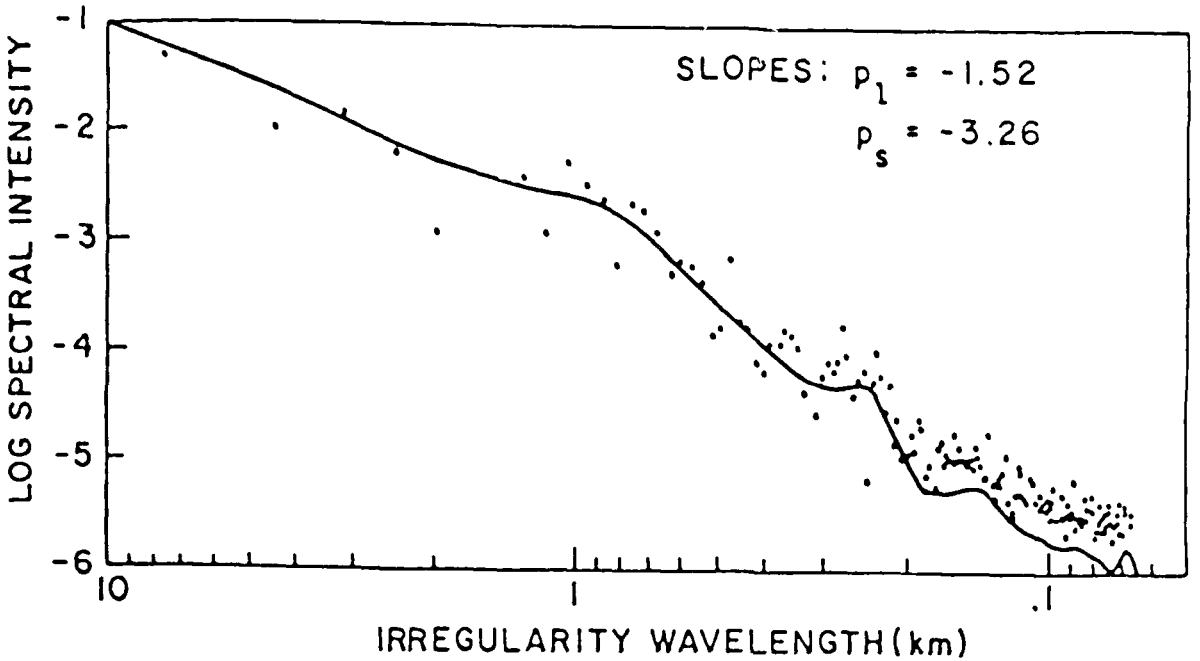

AE-E	22759
SIGMA %	13.694
NI	8.29E+05
ALT	436
SIN B.V	1.000
DIP	-27.64
LONG	-14.39
UT	003050

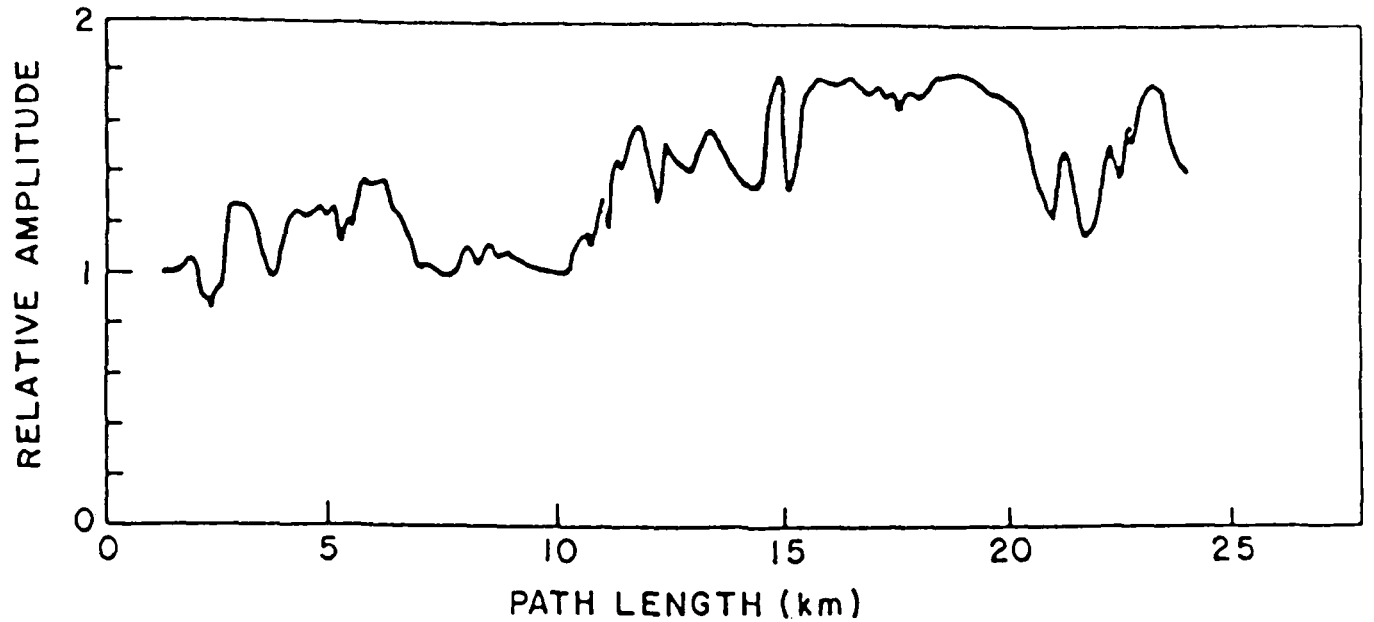

Figure 11

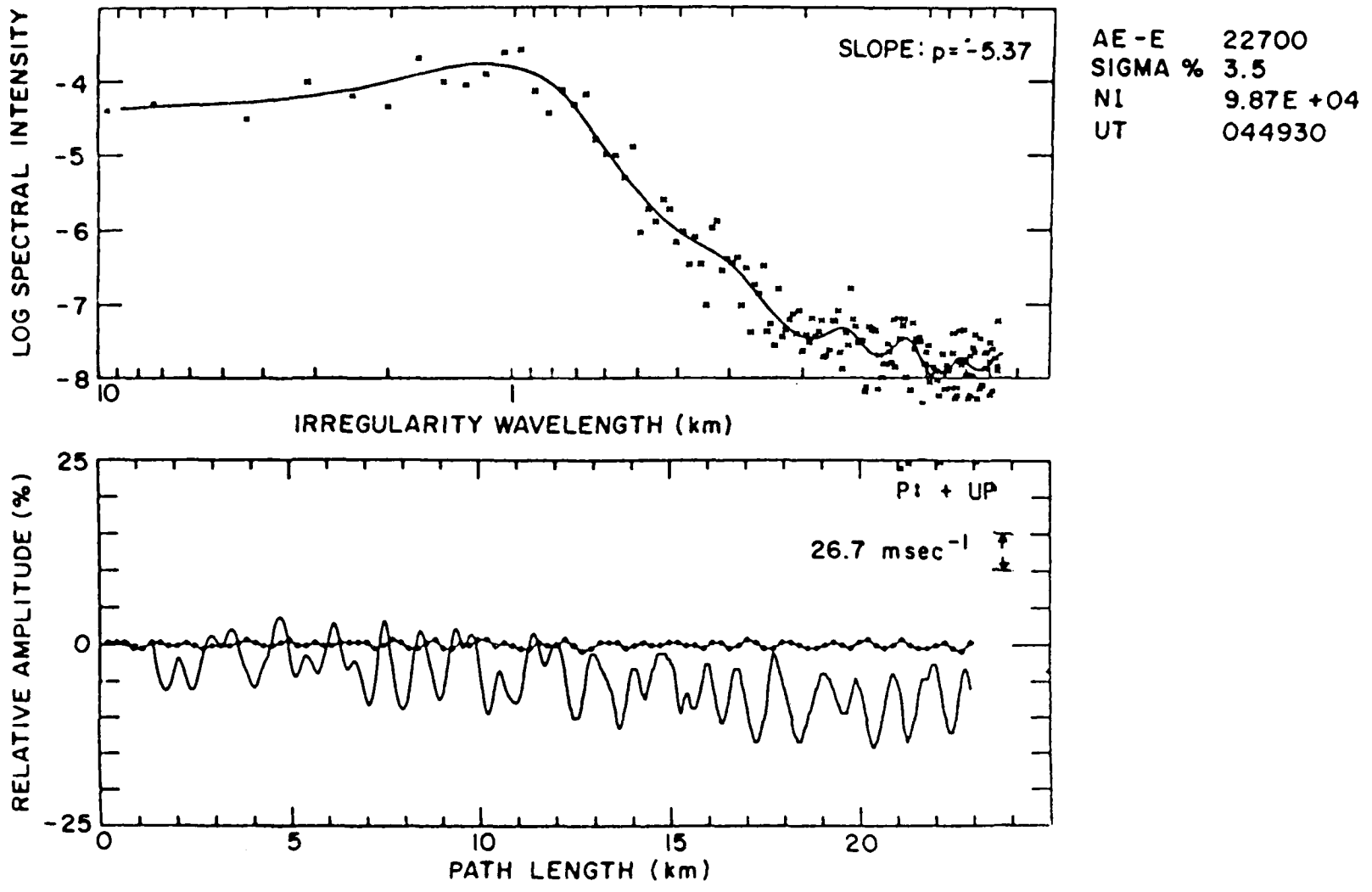
SLOPE: p= -5.37
AE -E 22700
SIGMA % 3.5
NI 9.87E +04
UT 044930
LOG SPECTRAL INTENSITY
-4
-5
-6
-7
-8
10
1
IRREGULARITY WAVELENGTH (km)
25
0
-25
RELATIVE AMPLITUDE (%)
P: + UP
26.7 msec⁻¹
0
5
10
15
20
PATH LENGTH (km)

Figure 12

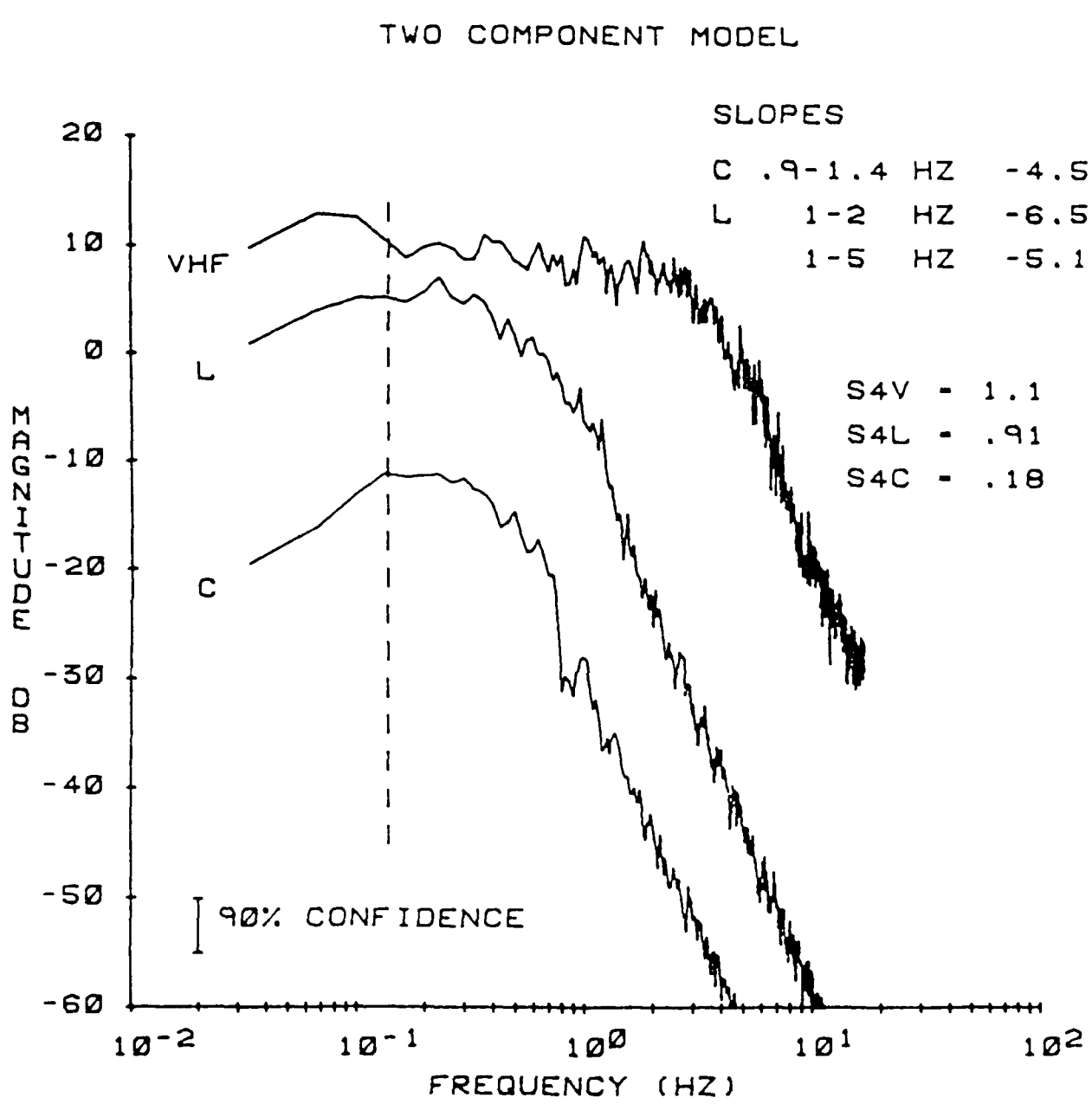
TWO COMPONENT MODEL
SLOPES
C .9-1.4 HZ -4.5 ±.7
L 1-2 HZ -6.5 ±.3
1-5 HZ -5.1 ±.1
S4V - 1.1
S4L - .91
S4C - .18
VHF
L
C
90% CONFIDENCE
MAGNITUDE DB
20
10
0
-10
-20
-30
-40
-50
-60
10-2
10-1
100
101
102
FREQUENCY (HZ)

Figure 13

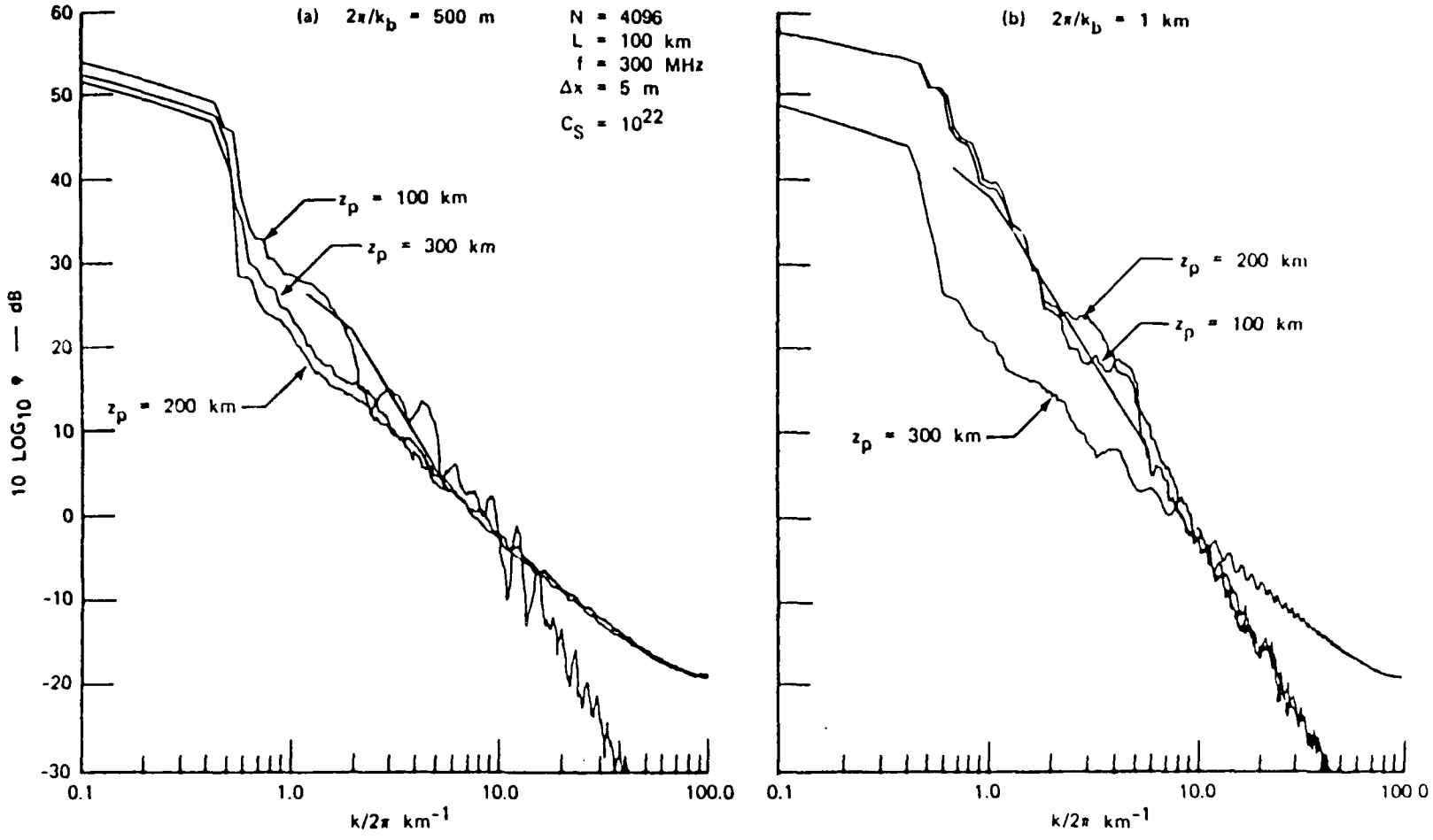

PHASE SPECTRA AT DIFFERENT PROPAGATION DISTANCES FOR TWO-COMPONENT POWER LAW

Figure 14

END

FILMED

7-85

DTIC